33rd Annual International Conference of the IEEE EMBS
Boston, Massachusetts USA, August 30 - September 3, 2011

# A Thermal Stereoscope for Surface Reconstruction of the Diabetic Foot

Matthew D. Parker, Andrew J. Taberner, Poul M. F. Nielsen

*Abstract*—**We have constructed a thermal stereoscope utilizing three digital SLR cameras and an infrared camera for rapid surface reconstruction of diabetic foot geometry and temperature distribution. A structured light pattern is projected on to the foot to provide approximately 2500 reconstructed points. The reconstructed point cloud is then fitted to a finite element model, producing root mean squared errors of less than 0.4 mm.**

## I. Introduction

Predictive biomechanical models of the foot need to accurately represent individual-specific surface geometry and underlying anatomy. This is especially an issue for diabetes patients who have foot deformities due to neuropathy and/or amputations [1-8]. In such cases the biomechanics of the foot are generally severely compromised and accurate analysis of loading is critical for optimising subsequent treatment and development of appropriate orthotic devices. While detailed anatomical information can be obtained from the analysis of magnetic resonance (MR) images of individuals, such approaches are too time-consuming and too costly to be used routinely in the clinic.

Neuropathy leads to loss of both sensation and control. This has significant consequences for diabetes sufferers who characteristically develop neuropathy, especially peripheral neuropathy in the feet. The loss of sensation removes the primary mechanism that alerts individuals to foot damage and infection – pain.

Nerve death also removes extrinsic control of foot muscles, resulting in further tissue and bone damage due to gait pathologies. Soft tissue inflammation often results from such infections and injuries. Although there is no pain felt by the individual, regions of tissue inflammation are often characterised by marked regional variations in skin surface temperature [9-13]. Current measurement systems monitor relatively few sites on the foot, or measure the temperature at the interface between the foot and a rigid platform.

Manuscript received April 15, 2011. This work was supported by the New Zealand Ministry of Research Science and Technology's New Economy Research Fund.

M. D. Parker is with the Auckland Bioengineering Institute at The University of Auckland (phone: +64 9 373 7599; fax: +64 9 367 7157 ; e-mail: mpar145@aucklanduni.ac.nz).

A. J. Taberner is with the Auckland Bioengineering Institute and the Department of Engineering Science at The University of Auckland (e-mail: a.taberner@auckland.ac.nz).

P. M. F. Nielsen is with the Auckland Bioengineering Institute and the Department of Engineering Science at The University of Auckland (e-mail: p.nielsen@auckland.ac.nz).

In order to characterize geometric and thermal changes in the diabetic foot in the clinical setting we propose the use of a multi-camera stereoscopic device that enables rapid, accurate, and inexpensive measurement of an individual's foot surface metrics, which will then be fitted to a finite element model.

## II. Methodology

### A. Design

The Stereoscopic rig consists of three digital SLR cameras (Canon 450D), providing 4272 x 2848 spatial resolution. Thermal data is gathered through a microbolometer-based thermal imager (Xenics Gobi-384), capable of 50 mK sensitivity. A 1080 x 720 video projector (PLUS U3-1080) is incorporated to readily provide various structured light routines. The cameras and projector are mounted to a rigid aluminum frame via Manfrotto ball-and-socket tripod heads.

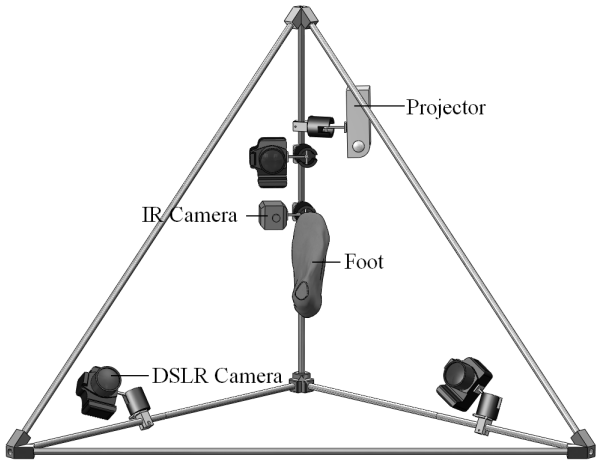


Fig. 1. Solidworks model of the thermal stereoscope rig. Unlabelled components refer to the aluminum support structure.

These tripod heads are free to slide along the aluminum rails, allowing versatility in imaging volumes.

Camera and projector control is operated via National Instruments' LabVIEW 2009. DSLR properties are adjusted via USB, while focus and shutter control are hardware-triggered using an NI USB-6008 data acquisition board, sending synchronized digital signals to each DSLR's dedicated triggering jack. The IR camera is currently software-triggered via a gigabit ethernet connection, but can also be hardware-triggered using a CameraLink interface.

*B. Structured Light*

An initial structured light routine based on Morano's pseudorandom (PR) array [14] has been used, in order to demonstrate the performance of the stereoscope.

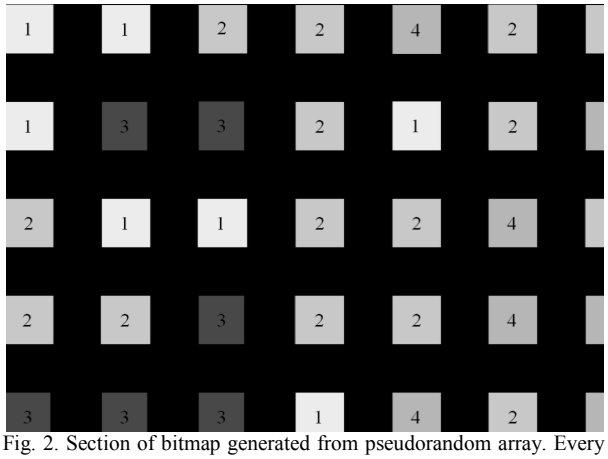


Fig. 2. Section of bitmap generated from pseudorandom array. Every three by three block of color-subunits appears only once in the entire array. Note: numbers are superimposed to differentiate grayscale and do not appear in the projected pattern.

A 225 x 106 PR array, of alphabet length = 4 has been constructed where every 3 x 3 sub-array appears only once. Each number in the alphabet is assigned a color, and a pixel map is constructed accordingly (Fig. 2). Each element in the array is represented by a single pixel, and separated from its neighboring elements by a two-pixel thick border of black.

The PR array encapsulates all coding data in a single projection, allowing imaging of a moving subject, which may be expected from a subject's foot.

Code extraction is performed in LabVIEW 2009, using the Vision toolkit. Images are thresholded via RGB or HSV channels, extracting a set of uniform-intensity particles for each color in the original PR array. Particle morphology studies are performed to estimate the sizes of particles and the location of their centroids. From this information the following steps are performed:

1. Discard particles outside the expected size
2. Locate the 8 closest neighbors for each particle (edge to edge)
3. Arrange the particle and its 8 closest neighbors into a fixed-order array (i.e. [top left, top center, top right, …, bottom left, bottom centre, bottom right]
4. Determine the location of the same sub-array in the remaining views.

*C. Camera Calibration*

The cameras, including the microbolometer were calibrated using Svoboda's multicamera calibration algorithm [15] This method does not require any predetermined metrics, and simply relies on projective geometry calculated between camera views of a bright spot moved throughout the imaging volume. A bright spot was constructed from a light emitting diode housed in a 3D-printed acrylonitrile butadiene styrene (ABS) sphere. Containing the LED in the sphere produces a visible signature for both IR and SLR cameras, where the centroid of the bright spot can be calculated accurately from multiple views.

The above camera calibration calculates the camera projection matrices from which two-dimensional image coordinates can be converted into three-dimensional world coordinates

*D. Geometric and Thermal Reconstruction*

Lines in space are back-projected from each camera center, through each set of image coordinates identified by the specific PR codewords. A world point is then defined at the intercept of these lines, or the point in space that minimizes the distance to each line (in the case of noise).

The PR pattern is not visible to the IR camera, so points are reconstructed using the DSLRs. Reconstructed world points are then forward projected through the IR camera center. Temperature values are read where the forward-projected line hits the IR image plane, and are assigned to the world point.

*E. Finite Element Modeling*

The reconstructed point cloud was fitted using a finite element model of the foot, developed at the Auckland Bioengineering Institute. This model was an extension of a surface mesh, generated from the NIH Visible Human Project dataset.

Data points were projected orthogonally on to the plantar surface of the foot if they lay within the bounds of a surface element, or projected non-orthogonally to the edge of the closest face. Fitted results were inspected for obviously abnormal geometry. Fitting was started again, with the affected nodes fixed in their original position. Fitting iterations were performed until the RMS distance between the fitted surface and the original data converged.

A similar method was applied to fit the temperature distribution. A uniform temperature field was set over the entire surface of the model. This value was set to 0 ºC, so as to clearly discriminate between data-rich/poor elements.

Fig. 3. Two views of a reconstructed point cloud of the foot.

## III. Results

### A. Foot Reconstruction

A healthy subject's foot was reconstructed from a single set of images (Fig. 3), producing approximately 2,500 points, at a point-to-point separation of 2 mm. A loss of data is evident around the toes.

### B. Model Fitting

A finite element model converged on the same point cloud after 7 iterations, producing an RMS error of approximately 0.39 mm. From Fig. 4 it can be seen that the lack of data around the toes has led to relatively poor reconstruction in this region.

Fig. 4. Face-fitted finite element model of a healthy subject's foot displaying surface geometry.

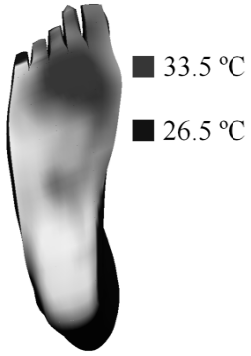


Fig. 5. Face-fitted finite element model of a healthy subject's foot displaying surface geometry and temperature distribution. Note hotter regions on the plantar surface appear darker.

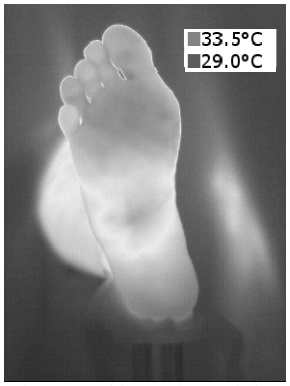


Fig. 6. Original IR image. White regions of the plantar surface are approximately 31 ºC.

Fig. 5 demonstrates a fitted temperature field to the geometry-fitted finite element model. This can be qualitatively compared to the false-colored original IR image of the foot (Fig. 6).

### C. Preliminary Validation

Two crosshairs with a separation of 50 mm were printed on white paper and attached to a 10 mm thick acrylic sheet. This system was assumed to be planar. The crosshairs were first placed within the plane at which the surface of the foot was expected to lie. The acrylic sheet was then tilted about a horizontal axis in 10º increments. At each position, a LabVIEW program extracted the centre of the crosshairs and triangulated their locations, providing an estimate of their separation in space. The same procedure was performed where the acrylic sheet was rotated about a vertical axis. By using printed crosshairs, the performance of the stereoscope could be investigated without the influence of the structured light routine, which is not intended to be the final projection pattern.

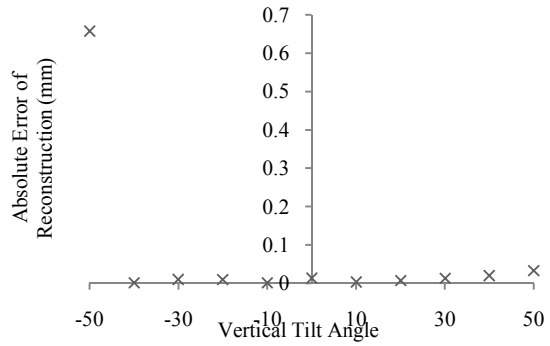


Fig. 7. Absolute error or reconstruction vs. vertical tilting for coplanar crosshairs

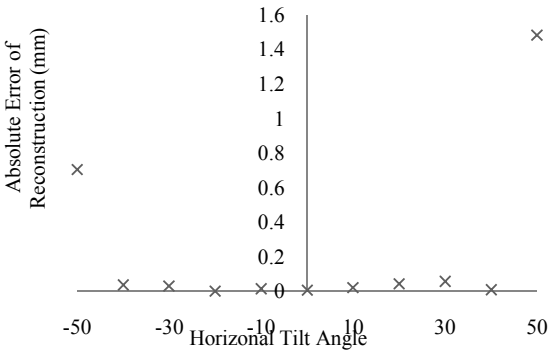


Fig. 8. Absolute error or reconstruction vs. horizontal tilting for coplanar crosshairs

Both Horizontal and Vertical tilting produced absolute errors in crosshair distance under 100 µm, over a range of 80º. Errors increase dramatically beyond ±40º in both orientations.

As the foot has a curved surface, planar validations cannot accurately gauge the performance of the stereoscope. Instead, a 55 mm radius PVC cylinder was constructed under the illumination of the PR light scheme. Reconstructions were made with the cylinder axis in both

horizontal and vertical orientations. Reconstruction performance was evaluated by cylindrical least squares fitting in MATLAB, using the Least Squares Geometric Elements library from EUROMETS, providing an estimated radius and RMS error of the data relative to the estimated

TABLE I
CYLINDER RECONSTRUCTION

| Cylinder Orientation | Estimated Radius (mm) | RMS error (mm) |
|---|---|---|
| Horizontal | 55.0094 | 0.0267 |
| Vertical | 55.0074 | 0.0278 |

Curved-surface validation by reconstruction of a PVC cylinder (Radius = 55mm). Orientations reflect the alignment of the cylinder axis.

radius. Both horizontal and vertical orientations of the cylinder provided accurate estimates up to the known resolution of the cylinder.

## IV. DISCUSSION

The preliminary results of the thermal stereoscope indicate promise for its application in a clinical environment. Over an 80º range, metrics were estimated to within 0.2%. These metrics suit the imaging profile of the diabetic foot, as most neuropathic ulcers appear on the plantar surface of the foot [16]. However, a wider range of surface orientations may be accurately reconstructed if more cameras are added to the periphery of the stereoscope.

Structured light routines can be expected to degrade the accuracy measure, though the use of Morano's PR array provided sub-millimeter-accurate estimates of a curved, featureless surface. A large fraction of the projected codes were lost beyond the border of the foot. Furthermore, this lighting approach broke down around the borders of the toes, due to high depth discontinuities and occlusion from the ball of the foot. Alternative methods, such as Zhang's multi-pass dynamic programming approach may resolve this issue [15].

The current point cloud density provides similar resolution to that used in MR-generated finite element meshes used in the diabetic foot literature [7,8]. As the stereoscope requires a single calibration for multiple reconstructions, and relies on a single image set per reconstruction, it has the potential to reduce turnaround times in the clinic.

The inclusion of an IR camera provides a high resolution, novel description of surface temperature distribution. This non-contact measurement approach may have advantages over previous methods, as the entire plantar surface of the foot can be measured.

Further investigation is required to validate the stereoscope's performance throughout the working volume and its ability to image highly varying surfaces. A quantitative evaluation of temperature fitting is also to be performed.

## REFERENCES


[1] Lemmon, D., Shiang, T .Y., Hashmi, A., Ulbrecht, J.S., & Cavanagh, P. R. 1997. The Effect of Insoles in Therapeutic Footwear-A Finite Element Approach. *J. biomechanics*, **30**(6), 615-620

[2] Erdemir, A., Saucerman, J. J., Lemmon, D., Loppnow, B., Turso, B., Ulbrecht, J.S., & Re, P. 2005. Local plantar pressure relief in therapeutic footwear : design guidelines from finite element models. *Journal of biomechanics*, **38**, 1798-1806J.

[3] Loppnow, B.W. 1999. The effect of plugs on reducing pressure under the second metatarsal head. M.s. thesis, The Pennsylvania State University, University Park, PA.

[4] Chen, W-P., Tang, F-T., & Ju, C-W. 2001. Stress distribution of the foot during mid-stance to push-off in barefoot gait: a 3-D finite element analysis. *Clinical biomechanics*, **16(**7), 614-620.

[5] Gefen, A. 2003. Plantar soft tissue loading under the medial metatarsals in the standing diabetic foot. *Medical engineering & physics*, **25**(6), 491-499.

[6] Thomas, V. J., Patil, K. M., & Radhakrishnan, S. 2004. Three-dimensional stress analysis for the mechanics of plantar ulcers in diabetic neuropathy. *Medical & biological engineering & computing,* **42**(2), 230-5.

[7] Cheung, J., Zhang, M., Leung, A., & Fan, Y. 2005. Three-dimensional finite element analysis of the foot during standing{a material sensitivity study. *Journal of biomechanics*, **38**(5), 1045-54.

[8] Dai, X., Zhang, M., & Cheung, J.T. 2006. Effect of sock on biomechanical responses of foot during walking. *Clinical biomechanics*, **21**(3), 314-321.

[9] Armstrong, D.G., Lavery, L.A., Liswood, P.J., Todd, W.F., & Tredwell, J.A. 1997a. Infrared Dermal Thermometry for the High-Risk Diabetic Foot. *Physical therapy*, **77**(2).

[10] Benbow, S. J., Chan, A .W., Bowsher, D. R., Williams, G., & Macfarlane, I. A. 1994. The prediction of diabetic neuropathic plantar foot ulceration by liquid-crystal contact thermography. *Diabetes care*, **17**(8), 835-9.

[11] Lavery, L. A., Higgins, K.R., Lanctot, D.R., & Constantinidies, G.P. 2007. Preventing Diabetic Foot Ulcer Recurrence Use of temperature monitoring as a self-assessment tool. *Diabetes care,* **30**(1), 14-20.

[12] Stess, R. M., Sisney, P. C., Moss, K. M., Graf, P. M., Louie, K. S., Gooding, G .A., & Grunfeld, C. 1986. Use of liquid crystal thermography in the evaluation of the diabetic foot. *Diabetes care*, **9**, 267-72.

[13] Sun, P., Lin, H., Jao, S. E., Ku, Y., Chan, R., & Cheng, C. 2006. Relationship of skin temperature to sympathetic dysfunction in diabetic at-risk feet. *Diabetes research and clinical practice*, **73**, 41-46.

[14] Morano, R.A., Ozturk, C., Conn, R., Dubin, S., Zietz, S., & Nissanov, J. 1998. Structured Light Using Pseudorandom Codes. *IEEE transactions on pattern analysis and machine intelligence*, **20**(3), 322-327.

[15] Svoboda, T., Martinec, D., & Pajdla, T. 2005. A Convenient Multicamera Self-Calibration for Virtual Environments. *Presence: Teleoperators & virtual environments*, **14**(4), 407-422.

[16] Laing, P. 1994. Diabetic foot ulcers. *American journal of surgery*, **167**(1A), 31S-36S.

[17] Zhang, B. Curless, S. M. Seitz, Rapid shape acquisition using color structured light and multi-pass dynamic programming, *Int. Symposium on 3D Data Processing Visualization and Transmission*, Padova, Italy, 2002.